ELSEVIER

Computers in Biology and Medicine 38 (2008) 694–708

Computers in Biology and Medicine

www.intl.elsevierhealth.com/journals/cobm

Finite element modeling of cooled-tip probe radiofrequency ablation processes in liver tissue☆

Rimantas Barauskas[a], Antanas Gulbinas[b], Tomas Vanagas[c], Giedrius Barauskas[c,*]

[a]*Department of System Analysis, Kaunas University of Technology, Kaunas, Lithuania*
[b]*Institute for Biomedical Research, Kaunas University of Medicine, Kaunas, Lithuania*
[c]*Department of Surgery, Kaunas University of Medicine, Eiveniu str. 2, LT-50009 Kaunas, Lithuania*

Received 13 November 2006; accepted 18 March 2008

Abstract

Finite element model of radiofrequency ablation (RFA) with cooled-tip probe in liver has been developed by employing *COMSOL Multiphysics* software. It describes coupled electric, thermal and sodium chloride solution infiltration flow phenomena taking place during ablation processes. Features of hydraulic capacity, saturation of the tissue by infiltration, and dependency of electrical conductivity on the damage integral of the tissue have been supplied to the model. RFA experiments have validated the model. Physical parameters describing hydraulic capacity and hydraulic conductivity in the tissue, as well as, the relation of electrical conductivity against the value of damage integral have been determined.

Keywords: Radiofrequency ablation; Computational modeling; Hydraulic conductivity; Experimental research

1. Introduction

The substantial proportion of patients with primary or metastatic malignancies confined to the liver are not candidates for resection because of tumor size, location, multifocal character or inadequate functional hepatic reserve [1]. Radiofrequency ablation (RFA), a local thermal ablative technique for the treatment of unresectable hepatic tumors including hepatocellular carcinoma, proved to be tumoricidal [2].

RFA takes place at frequencies 460–550 kHz. Electrical voltage is being applied to the ablation zone by means of an electrically active probe. The flow of electrical current transfers the energy to the tissue, and the temperature there reaches 100 °C during time interval of 10–15 min [3,4]. The basic physical processes taking place during RFA are the electrical current flowing in the tissue and causing volumetric heat generation, as well as, the heat exchange due to thermal conductance of tissues. The electrical conductivity is dependent on the temperature of the tissue, therefore a coupled electro-thermal problem can be formulated [6]. RFA processes performed by using cooled-tip ablation probes are physically more complex because of the flow of sodium chloride (NaCl) solution injected through the active part of the ablation probe in order to prevent tissue carbonization, which may impede or even block the heat transfer into the tissue.

The infiltration flow of the injected solution makes a significant influence on the overall heat transfer process of RFA due to marked amount of heat energy transferred into the tissue by advection, which is the transport of heat by means of moving fluid. The heat power transferred by the fluid flow at each point of the tissue depends on the velocity of the fluid, therefore it has to be calculated by solving the hydraulic conductivity partial differential equations and further employed in the advection–diffusion equation, which describes the combined process of heat transfer. As a final result, the advection makes the heated zone wider spread and simultaneously the peak temperature in the nearest vicinity of the electrode is lower than in the case of purely conductive heat exchange. The heating of the tissue by high frequency electrical current together with the heat conductivity and advection mechanisms complete the

☆ The study was sponsored by the Lithuanian Science and Studies Foundation.

* Corresponding author. Tel.: +370 686 525 96; fax: +370 37 326 824.
E-mail addresses: rimantas.barauskas@ktu.lt (R. Barauskas), gulbanta@gmail.com (A. Gulbinas), giedrius.barauskas@gmail.com (G. Barauskas).

0010-4825/$ - see front matter © 2008 Elsevier Ltd. All rights reserved.
doi:10.1016/j.compbiomed.2008.03.007

full physical view of thermal processes to be taken into account in the mathematical description of RFA. In this way a fully coupled electrical, thermal and infiltration flow mathematical problem can be formulated. It is known that at 500 kHz frequency the electrical conductivity of liver tissue is approximately 0.148 1/Ωm [5], and it is determined mostly by the active electrical conductance. Therefore the analysis can be reasonably simplified by assuming the equations of electric phenomena formulated in terms of steady amplitudes of electric voltage and current, subsequently the electric power being expressed as the product of the effective values of voltage and current. This implies the consideration of alternating voltage and electrical current in terms of their effective values obtained by solving the equations of direct current in conductive media. Models of such type have been employed during RFA processes modeling in [6,7]. The lesion of the tissue as a consequence of heating can be evaluated by using the *Arrhenius* formula [7].

During RFA processes *in vivo*, in addition to the heat conductance and heat advection by the flow of infiltrated solution, the heat advection takes place due to heat transport by the blood flow in liver tissue. The latter heat transfer mechanism is very complex due to non-uniform blood velocity field in the tissue and due to the presence of a dense net of blood vessels of varying calibers, which may sewer considerable amount of heating energy. Most of the research works published up to now employ simplified approaches for taking into account heat losses in the RFA zone due to advection. Chang and Nguyen [6,7] have employed a perfusion coefficient to take into account volumetric heat losses due to thermal power absorbed by the blood. Neither blood nor the NaCl solution velocities were employed in the equations explicitly.

Extensive experimental work and adjustment of RFA procedures are often performed on *ex vivo* biological tissues. A basic distinguishing feature of RFA process performed on an *ex vivo* tissue is the absence of blood perfusion and smaller amount of interstitial fluid. Though cadaveric liver tissue contains ~ 77% of water [8], significant extra volume of fluid can be infiltrated and absorbed by intercellular space.

In this study mathematical model of RFA ablation in liver tissues has been developed. As a novel feature of the model, the coupling of the electrical–thermal conductivity problem with the heat advection by means of the infiltrated flow velocity field, which is caused by the injection of NaCl solution through the RFA probe, has been described. The infiltration process is modeled by employing the approach presented recently by our group [9] assuming the flow being similar to Darcy's flow of the fluid through porous media. The role of the "pores" in the liver tissue is played by intercellular spaces and small empty blood vessels. The model is supplemented with the nonlinear hydraulic capacity term, which evaluates the possibility of cadaveric tissue to accommodate certain volume of fluid within its intercellular volume until the saturation point is reached. The amount of accommodated fluid volume is expressed in terms of volumetric saturation fraction (VSF). The overall model is enhanced by introducing the nonlinear relationship of electrical conductivity of the tissue against its damage integral. The computations are followed by experimental validation of the model in cadaveric porcine liver.

2. Mathematical model

2.1. Problem formulation

The RFA process is initiated by the high frequency alternating voltage applied to the electrically conductive ablation probe inserted into tumor tissue. We investigate the RFA process initiated by a probe, the geometry of which resembles a hollow needle of diameter 0.002 m inserted into liver tissue 0.06 m deep. Only the tip of the probe of length 0.02 m is electrically active and serves as a conductor of electric current flowing into the tissue. It causes the distributed electrical current to flow through the tissue in the direction of the grounding electrode attached elsewhere to the patient's body. The distance between the probe and the grounding electrode is usually much larger than linear size of the probe, as well as, of the tumor. In order to obtain a finite element model of reasonable dimensions we investigate only a cylinder-shaped zone of the tissue of diameter 0.12 m in the vicinity of the probe insertion point, Fig. 1. The size of the investigated zone is selected freely in order to approximate the "nearly infinite" surrounding of the probe. To make sure that the finite size of the investigation zone did not introduce prohibitive errors of calculations, we may solve the same problem at this and at a larger domain size and to compare the obtained results. If the domain size is large enough, the obtained results should be approximately the same in both domains.

The electrical current flow through the tissue causes the volumetric heat generation. The heat is redistributed through the continua in time due to thermal conduction of the tissue and the advection heat transfer by means of the infiltrated NaCl solution. The NaCl solution is infiltrated into the tissue through eyeholes of the hollow ablation probe, fills in the intercellular spaces and spreads over the investigated liver zone.

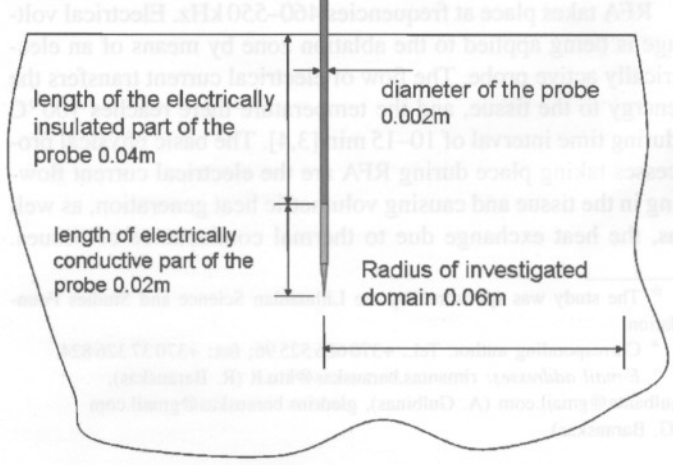

Fig. 1. Geometry of investigated axissymmetric domain.

The velocities of the fluid at each point of the zone are calculated by solving the fluid flow equations.

Therefore the overall physical process is determined by coupled electrical, thermal and hydraulic phenomena, most of which are nonlinear. The following mathematical formulation of the problem is presented for the axially symmetric domain, where the liver tissue is considered as homogeneous continua. In the following we discus all aspects of the model in more detail.

2.2. Electrical current

Applying a quasi-static model of electrical conductance we performed the analysis of distributed electrical current in liver tissues during RFA. The alternating voltage and electrical current in axially symmetric conductive continua are described in terms of their effective values by means of the equation

$$\frac{\partial}{\partial r}\left(2\pi r\sigma\frac{\partial\varphi}{\partial r}\right)+\frac{\partial}{\partial z}\left(2\pi r\sigma\frac{\partial\varphi}{\partial z}\right)=0,\quad \in V, \tag{1}$$

where φ is the electric potential (V), σ the electrical conductivity of the tissue ($1/\Omega$m), and r, z the radial and axial coordinates, (m).

Multiplier term $2\pi r$ appears in the equation due to axial symmetry of the domain and implies that integrals are calculated in the cylindrical system of coordinates. Therefore we cancel out neither multiplier 2π from Eq. (1) nor multiplier term $2\pi r$ from subsequent relations, which describe the boundary conditions. The expression $2\pi r\sigma$ could be rather interpreted as equivalent electrical conductivity coefficient used in axissymmetric formulation. Usage of equivalent conductivity values enables to calculate the integrals over flat triangle finite elements.

Cauchy (Neuman) boundary condition

$$2\pi r n_r\sigma\frac{\partial\varphi}{\partial r}+2\pi r n_z\sigma\frac{\partial\varphi}{\partial z}=0,\quad \in S_C^E \tag{2}$$

is used at the insulated boundary of the probe, at the free surface of the tissue and at the line of axial symmetry inside the tissue. The physical meaning of (2) is that no electrical field lines are leaving the domain through this boundary.

Dirichlet boundary condition

$$\varphi=\varphi_{\mathrm{E}},\quad \in S_D^E \tag{3}$$

is applied to the surface at the electrically active part of the probe (φ_{E} given) and to the external boundaries of the investigated domain situated "far enough" from the ablation probe ($\varphi_{\mathrm{E}}=0$), Fig. 2a.

2.3. Infiltration of fluid

During ablation processes in *ex vivo* tissues the only fluid flow in the tissue is due to the infiltration of the fluid. Assume that in the nearest vicinity of the ablation probe only small blood vessels exist. It is extremely difficult to take into account the influence of the blood vessels on the overall infiltration flow

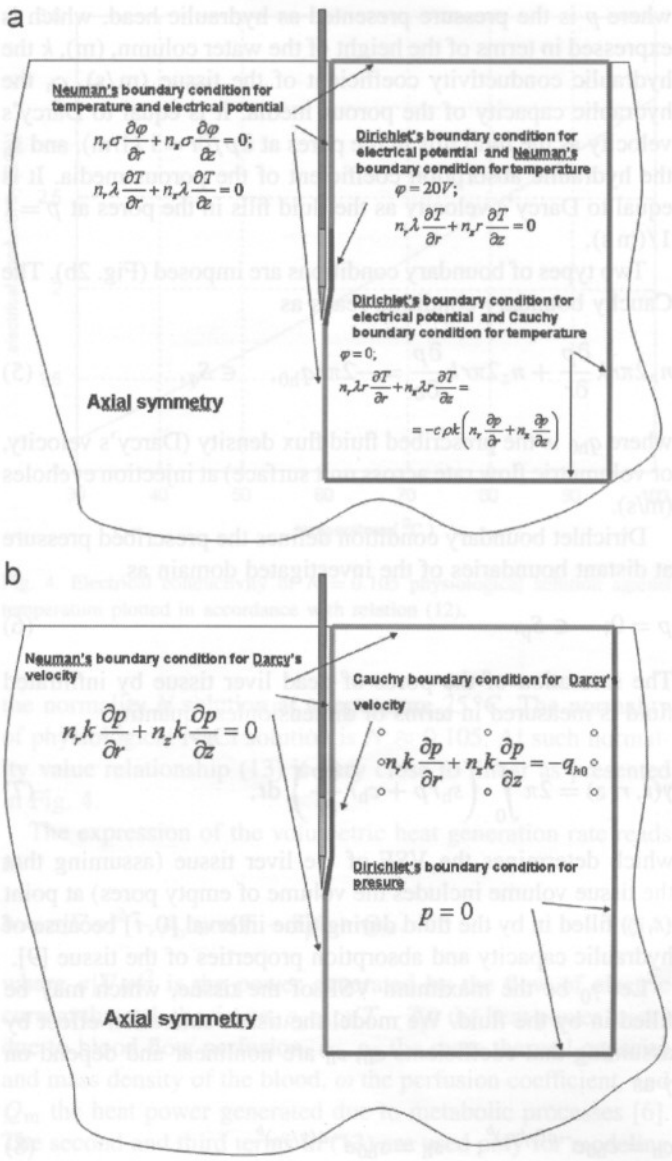

Fig. 2. Boundary conditions of the investigated domain: (a) infiltration flow; and (b) b—electrical and thermal.

exactly, therefore we are basing ourselves on the assumption that the infiltration flow can be approximately presented by the mathematical model of flow through porous tissue able to contain certain amount of fluid until the intercellular spaces and small blood vessels are saturated. The values of physical constants of the mathematical model were determined in our earlier work [9] by comparing computational results with the results of carefully planned experiments.

Further we assume that the infiltration of NaCl solution into the liver tissue during RFA process is described by using the hydraulic conductivity equation based on Darcy's law [10]:

$$\frac{\partial}{\partial r}\left(2\pi r k\frac{\partial p}{\partial r}\right)+\frac{\partial}{\partial z}\left(2\pi r k\frac{\partial p}{\partial z}\right)$$
$$=2\pi r s_{\mathrm{h}}p+2\pi r c_{\mathrm{h}}\frac{\partial p}{\partial t},\quad \in V, \tag{4}$$

where p is the pressure presented as hydraulic head, which is expressed in terms of the height of the water column, (m), k the hydraulic conductivity coefficient of the tissue (m/s), c_h the hydraulic capacity of the porous media. It is equal to Darcy's velocity as the fluid fills in the pores at $\partial p/\partial t = 1$ (1/m), and s_h the hydraulic absorption coefficient of the porous media. It is equal to Darcy's velocity as the fluid fills in the pores at $p = 1$ 1/(m s).

Two types of boundary conditions are imposed (Fig. 2b). The Cauchy boundary condition reads as

$$n_r 2\pi rk\frac{\partial p}{\partial r} + n_z 2\pi rk\frac{\partial p}{\partial z} = -2\pi r q_{h0}, \quad \in S_q, \tag{5}$$

where q_{h0} is the prescribed fluid flux density (Darcy's velocity, or volumetric flow rate across unit surface) at injection eyeholes (m/s).

Dirichlet boundary condition defines the prescribed pressure at distant boundaries of the investigated domain as

$$p = 0; \quad \in S_p. \tag{6}$$

The saturation of the pores of dead liver tissue by infiltrated fluid is measured in terms of dimensionless quantity

$$\gamma(\tilde{t}, r, z) = 2\pi \int_0^{\tilde{t}} \left(s_h r p + c_h r \frac{\partial p}{\partial t} \right) \mathrm{d}t, \tag{7}$$

which determines the VSF of the liver tissue (assuming that the tissue volume includes the volume of empty pores) at point (r, z) filled in by the fluid during time interval $[0, \tilde{t}]$ because of hydraulic capacity and absorption properties of the tissue [9].

Let γ_0 be the maximum VSF of the tissue, which may be filled in by the fluid. We model the tissue saturation effect by assuming that coefficients c_h, s_h are nonlinear and depend on γ as

$$c_h = c_{h0} e^{-a(\gamma/\gamma_0)^b}; \quad s_h = s_{h0} e^{-a(\gamma/\gamma_0)^b}. \tag{8}$$

At coefficient values $a = 3.815$ and $b = 6$ the relationship presented in Fig. 3 is obtained.

The presented fluid infiltration into the liver tissue model does not pretend to be correct in the vicinity of large blood vessels. In such cases the geometry and hydraulic capacities of the particular blood vessels should be directly included into the finite element model.

2.4. Thermal phenomena

Thermal field in the tissue is described by the heat diffusion-advection equation as

$$\frac{\partial}{\partial r}\left(2\pi r\lambda\frac{\partial T}{\partial r}\right) + \frac{\partial}{\partial z}\left(2\pi r\lambda\frac{\partial T}{\partial z}\right) + 2\pi rc\rho k\frac{\mathrm{d}p}{\mathrm{d}r}\frac{\mathrm{d}T}{\mathrm{d}r} + 2\pi rc\rho k\frac{\mathrm{d}p}{\mathrm{d}z}\frac{\mathrm{d}T}{\mathrm{d}z} + 2\pi rb(r,z) = 2\pi r\rho c\frac{\partial T}{\partial t}, \quad \in V, \tag{9}$$

where T is the temperature of the tissue (K), b the volumetric density of heat source (W/m^3), λ the thermal conductivity

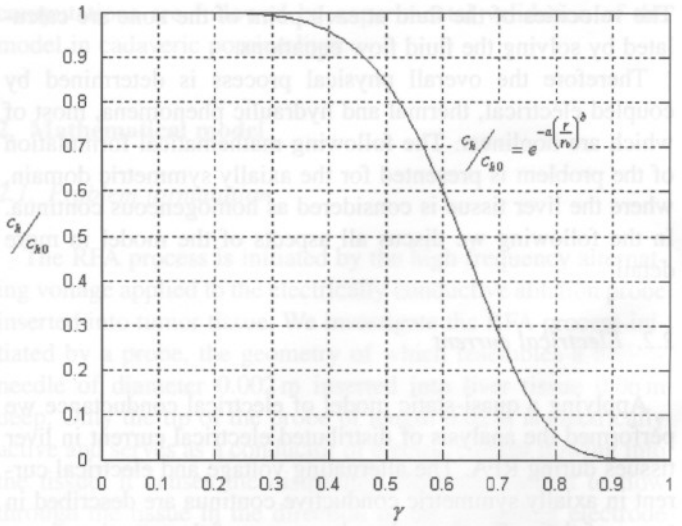

Fig. 3. Relationship of relative hydraulic capacity coefficient against the volumetric fraction of tissue filled in by the fluid (saturation point $\gamma_0 = 0.84$, $a = 3.815$, $b = 6$).

(W/(K m)), c the mass thermal capacity (J/(K kg)), and ρ the mass density (kg/m^3), terms $-k_x(\mathrm{d}p/\mathrm{d}x)$; $-k_y(\mathrm{d}p/\mathrm{d}y)$ are the components of Darcy's velocity of NaCl solution injected through the eyeholes of the ablation probe and flowing into the intercellular spaces of the tissue.

Cauchy boundary condition defines the thermal exchange with the environment of the investigated domain as

$$2\pi rn_r\lambda\frac{\partial T}{\partial x} + 2\pi rn_z\lambda\frac{\partial T}{\partial z} + 2\pi rq + 2\pi r\alpha(T - T_\infty) = 0, \quad \in S_C^T, \tag{10}$$

where α is the film coefficient (W/K m^2), T_∞ the temperature of the environment (K), and q the prescribed heat flux density across the surface (W/m^2). Eq. (10) includes two physically different boundary conditions. Term $2\pi rq$ indicates a prescribed thermal flux density across the boundary, and term $2\pi r\alpha(T - T_\infty)$ describes thermal flux density across the boundary surface due to heat exchange across the interface between two environments. Therefore q and α cannot be non-zero at the same part of the surface.

In our model the last term of (10) is never used as practically heat exchange across the outer interface between the tissue and air may be assumed as negligible. Value $q = 0$ in (10), which means the thermal isolation of the investigated domain at the boundary, is used instead at the boundaries with the air and with the ablation probe, as well as, at the boundary of the axial symmetry.

Expression $q = c\rho k(n_r(\partial p/\partial r) + n_z(\partial p/\partial z))$ in (10), which means the heat flux transported out of the domain by the fluid flow, is used at the distant boundaries (Fig. 2a):

$$2\pi rn_r\lambda\frac{\partial T}{\partial x} + 2\pi rn_z\lambda\frac{\partial T}{\partial z} = -2\pi rc\rho k\left(n_r\frac{\partial p}{\partial r} + n_z\frac{\partial p}{\partial z}\right), \quad \in S_C^T. \tag{10'}$$

As an alternative, the Dirichlet boundary condition

$$T = T_p, \quad \in S_D^T, \tag{11}$$

may be used for defining the known temperature of the tissue at distant boundaries, where $T_p = 310\,\mathrm{K} = 37\,^\circ\mathrm{C}$. However, as observed in our calculations, the performance of the nonlinear model was more robust when we used boundary condition (10) at distant boundaries rather than boundary condition (11). Practically, in some situations the global solution process even failed to converge if boundary condition (11) was employed. Both boundary conditions alternatives $(10)'$ and (11) physically do not contradict to each other. As only one of them is necessary to use, we chose an easier way and carried out our analyses by using $(10)'$.

2.5. Damage of the tissue

The damage of the tissue due to heating is obtained by *Arhenius* formula [7], which defines the value of the "damage integral" as

$$\Omega(t) = \ln \frac{c(0)}{c(t)} = A \int_0^T \mathrm{e}^{-\Delta E/RT(t)}\,\mathrm{d}t, \tag{12}$$

where $c(t)$ is the concentration of live cells, R the universal gas constant, A the "frequency" coefficient (s^{-1}), and ΔE the energy of initiation of irreversible ablation reaction (J/mol).

Parameters A and ΔE have been characterized for liver tissues [11]. Damage integral value $\Omega = 1$ corresponds to 63% probability of cell death at a specific point, and value $\Omega = 4.6$ corresponds to 99% probability of cell death at a point in the model. The significance of $\Omega = 1$ has been reported as the point at which tissue coagulation first occurs [12].

2.6. Coupling of multiphysical phenomena

The coupling of the electric and thermal fields takes place due to the dependency of the electrical conductivity σ in Eq. (1) on the temperature of the tissue and due to the volumetric heat generation rate the magnitude of which is dependent on the electric current strength. Values of electrical conductivity of liver tissues at different temperatures are not comprehensively investigated at the time being. In practical calculations the electrical conductivity of the tissue is usually identified with the electrical conductivity $\sigma(T, N)$ of NaCl solution of normality N and temperature T (°C), which has been expressed by Strogyn [13] as

$$\begin{aligned}\sigma(T, N) = {} & \sigma(25, N) * (1.000 - 1.962\mathrm{e}-2 * (25 - T) \\ & + 8.08\mathrm{e}-5 * (25 - T).^2 - \cdots \\ & \times N * (25 - T). * (3.020\mathrm{e}-5 + 3.922\mathrm{e} \\ & - 5 * (25 - T) + N * (1.721\mathrm{e}-5 * (25 - T) \\ & - 6.584\mathrm{e}-6 * (25 - T)))),\end{aligned} \tag{13}$$

where $\sigma(25, N) = N * (10.394 - 2.3776 * N + 0.68258 * N^2 - 9.13538 * N^3 + 1.0086\mathrm{e}{-2} * N^4)$ is the electrical conductivity of the normality N solution at temperature 25 °C. The normality of physiological NaCl solution is $N \approx 0.105$. At such normality value relationship (13) is very close to linear as presented in Fig. 4.

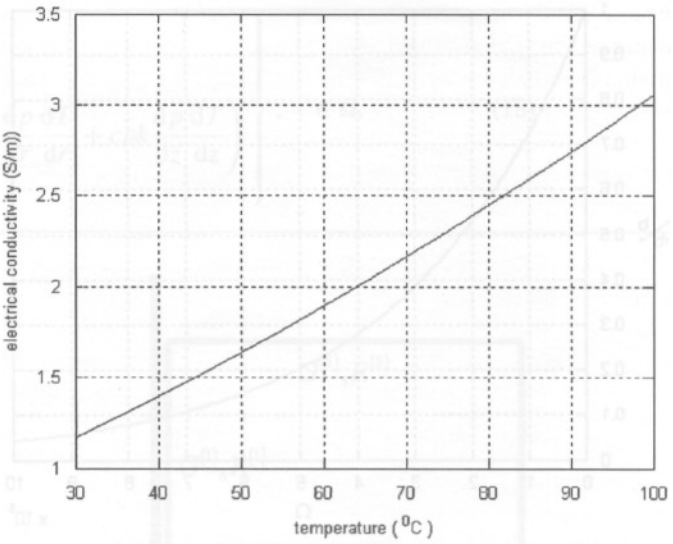

Fig. 4. Electrical conductivity of $N = 0.105$ physiological solution against temperature plotted in accordance with relation (12).

The expression of the volumetric heat generation rate reads as

$$b = \sigma|\nabla\varphi|^2 - \rho_b c_b \omega(T - T_p) + Q_m, \tag{14}$$

where $\sigma|\nabla\varphi|^2$ is the power generated by the flow of electric current through the tissue, $\rho_b c_b \omega(T - T_p)$ the heat power losses due to blood flow perfusion, c_b, ρ_b the mass thermal capacity and mass density of the blood, ω the perfusion coefficient, and Q_m the heat power generated due to metabolic processes [6]. The second and third terms in (13) are used only for modeling the RFA processes in live tissue.

Our investigations demonstrated that the dependence of electrical conductivity of the tissue against its damage integral Ω has to be taken into account by scaling tissue electrical conductivity as

$$\tilde{\sigma} = \sigma \times 1.1^{\Omega/300\,000}, \tag{15}$$

where σ is obtained from (13).

Relationship (15) is graphically presented in Fig. 5. As direct experimental measurement data were not available, the parameters of the relationship σ against Ω have been adjusted in order to ensure the best match of computed and experimental time laws of tissue temperature. A thorough discussion on this point is presented in Section 3 of this paper.

The coupling of the thermal and fluid flow fields is ensured by advection terms in Eq. (9). In addition, the fluid flow has the influence upon the coefficients used in both electrical and thermal equations because of the following considerations. As the research is concentrated upon RFA processes taking place in *ex vivo* setting, the partial dehydration of tissue has to be

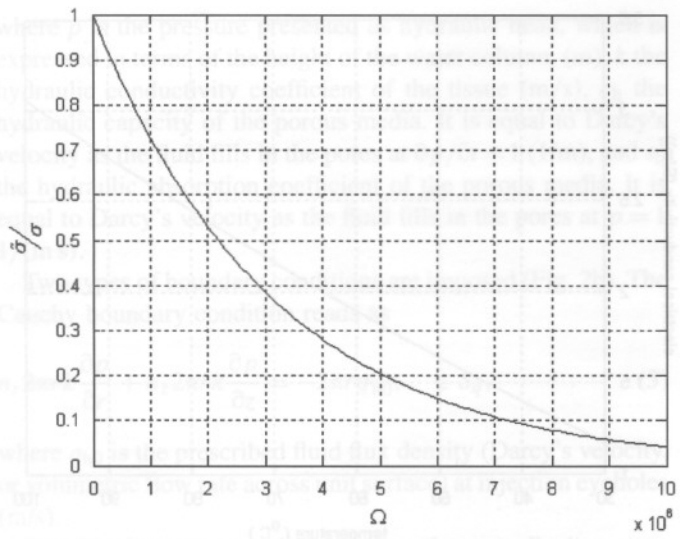

Fig. 5. Relationship of electrical conductivity of the tissue against the damage integral.

Table 1
The values of physical constants

Temperature of surrounding tissues	$T_p = 310\,\mathrm{K}$
Mass density of tissues	$\rho = 1060\,\mathrm{kg/m^3}$
Thermal conductance of tissues	$\lambda = 0.5020\,\mathrm{W/K\,m}$
Thermal capacity of tissues	$c = 3600\,\mathrm{J/kg\,K}$
Electrical conductivity of tissues	$\sigma = 0.148\,1/\Omega\mathrm{m}$
Mass density of blood	$\rho_b = 1000\,\mathrm{kg/m^3}$
Thermal capacity of blood	$c_b = 4180\,\mathrm{J/kg\,K}$
Perfusion coefficient	$\omega = 6.4e-3\,\mathrm{s^{-1}}$
"Frequency" coefficient	$A = 7.39 \times 10^{39}\,\mathrm{s^{-1}}$
Energy of initiation of irreversible ablation reaction	$\Delta E = 2.577 \times 10^5\,\mathrm{J/mol}$
Universal gas constant	$R = 8.314\,472(15)\,\mathrm{J/(mol\,K)}$

taken into account. Though the cadaveric tissue still contains ~ 77% of water [8], our experiments demonstrated that additional content of the solution comprising ~ 48% of cadaveric tissue volume can be infiltrated. Naturally, the process is followed by enlargement of the tissue volume subject to infiltration of appropriate volume of fluid. As in our model the process is investigated in the finite element mesh of fixed dimensions, it appears reasonable to treat the mesh as presenting the maximum possible volume of the tissue. At the same time the existence of empty "pores" is assumed, which are filled in by the solution as it is infiltrated into the tissue. Basing on the obtained data, the initial VSF of the fluid infiltrated into cadaveric tissue is $\gamma = 0.521$, and the maximum possible value of the VSF is $\gamma_0 = 0.84$. The influence of the VSF of filling in the pores upon conductivity coefficients, as well as, the mass density of the tissue should be considered. As a rough approximation, the coefficients k, λ and ρ are scaled by the quantity $1-\gamma_0+\gamma$ in Eqs. (1)–(5), (9) and (10).

The values of physical constants listed in Table 1 have been taken from [6]. Values of some other necessary but not available constants have been determined in the course of the model validation.

2.7. "General" form of equations in COMSOL Multiphysics computational environment

The computational realization of the full and complex coupling of the three fields in the considered multifield physical problem is hardly implementable in most general-purpose finite element software systems. The *COMSOL Multiphysics* is probably the best-suited software available today for implementing the task required in this investigation. It enables to generate a finite model of arbitrary complexity and coherency starting from the formulation posed in terms of partial differential equations. In *COMSOL* Multiphysics the partial differential Eqs. (1), (4), and (9) with boundary conditions Eqs. (2), (3), (5), (6), (10)′, (11), (2), and (3) relations (7) and (14) along with all above-discussed coupling terms are presented in the "general" form [14,15] as

$$d_a \begin{Bmatrix} \dot{\gamma} \\ \dot{p} \\ \dot{\varphi} \\ \dot{T} \\ \dot{\Omega} \end{Bmatrix} + \nabla \cdot \Gamma = F, \quad \in V, \tag{16}$$

with boundary conditions

$$\begin{cases} -\vec{\mathbf{n}} \cdot \Gamma = G, & \in S, \\ 0 = R, & \in S, \end{cases} \tag{17}$$

where

$$d_a = \begin{bmatrix} -1 & 2\pi r c_h & 0 & 0 & 0 \\ 0 & 2\pi r c_h & 0 & 0 & 0 \\ 0 & 0 & 0 & 0 & 0 \\ 0 & 0 & 0 & 2\pi r \rho c(1-\gamma_0+\gamma) & 0 \\ 0 & 0 & 0 & 0 & 1 \end{bmatrix};$$

$$\Gamma = -\begin{Bmatrix} \begin{bmatrix} 0 \\ 0 \end{bmatrix} \\ \begin{bmatrix} 2\pi r k \dfrac{\partial p}{\partial r} \\ 2\pi r k \dfrac{\partial p}{\partial z} \end{bmatrix} \\ \begin{bmatrix} 2\pi r \sigma(1-\gamma_0+\gamma)\dfrac{\partial \varphi}{\partial r} \times 1.1^{\Omega/300\,000} \\ 2\pi r \sigma(1-\gamma_0+\gamma)\dfrac{\partial \varphi}{\partial z} \times 1.1^{\Omega/300\,000} \end{bmatrix} \\ \begin{bmatrix} 2\pi r \lambda(1-\gamma_0+\gamma)\dfrac{\partial T}{\partial r} \\ 2\pi r \lambda(1-\gamma_0+\gamma)\dfrac{\partial T}{\partial z} \end{bmatrix} \\ 0 \end{Bmatrix};$$

$$F = \begin{Bmatrix} -2\pi r s_h p \\ -2\pi r s_h p \\ 0 \\ 2\pi r \left(\sigma \left(\dfrac{\partial \varphi}{\partial r} \right)^2 + \sigma \left(\dfrac{\partial \varphi}{\partial z} \right)^2 - \rho_b c_b \omega (T - T_p) + Q_m + c\rho k \dfrac{dp}{dr} \dfrac{dT}{dr} + c\rho k \dfrac{dp}{dz} \dfrac{dT}{dz} \right) \\ Ae^{-\Delta E/RT} \end{Bmatrix}, \quad \in \Omega. \tag{18}$$

G and R present five different boundary condition sets as

$$G^{(1)} = \begin{bmatrix} 0 \\ 0 \\ 0 \\ 0 \\ 0 \end{bmatrix}; \quad R^{(1)} = \begin{bmatrix} 0 \\ 0 \\ 0 \\ 0 \\ 0 \end{bmatrix};$$

$$G^{(2)} = \begin{bmatrix} 0 \\ 0 \\ 2\pi r c\rho k \left(n_r \dfrac{dp}{dr} + n_z \dfrac{dp}{dz} \right) \\ 0 \\ 0 \end{bmatrix}; \quad R^{(2)} = \begin{bmatrix} 0 \\ p - p_0 \\ \varphi_E \\ 0 \\ 0 \end{bmatrix};$$

$$G^{(3)} = \begin{bmatrix} 0 \\ 0 \\ 0 \\ 2\pi r c\rho q_{h0} (T - T_{in}) \\ 0 \end{bmatrix}; \quad R^{(3)} = \begin{bmatrix} 0 \\ 2\pi r q_{h0} \\ \varphi_E - \varphi_{E0} \\ 0 \\ 0 \end{bmatrix};$$

$$G^{(4)} = \begin{bmatrix} 0 \\ 0 \\ 0 \\ 0 \\ 0 \end{bmatrix}; \quad R^{(4)} = \begin{bmatrix} 0 \\ 0 \\ \varphi_E - \varphi_{E0} \\ 0 \\ 0 \end{bmatrix};$$

$$G^{(5)} = \begin{bmatrix} 0 \\ 0 \\ 0 \\ 0 \\ 0 \end{bmatrix}; \quad R^{(5)} = \begin{bmatrix} 0 \\ p - p_0 \\ 0 \\ 0 \\ 0 \end{bmatrix}, \tag{19}$$

which are applied to boundaries of the domain as indicated in Fig. 6,

$$c_h = c_{h0} e^{-a(\gamma/\gamma_0)^b}; \quad s_h = s_{h0} e^{-a(\gamma/\gamma_0)^b};$$
$$\gamma_0 = 0.84; \quad a = 3.815; \quad b = 6,$$

q_{h0} is the prescribed fluid flux density at the part of the probe supplied with infusion eyeholes; T_{in} the temperature of the fluid entering the domain through the eyeholes of the active part of the ablation probe; T_p the ambient temperature; p_0 the pressure prescribed on distant boundaries of the domain; and φ_{E0} the electrical potential prescribed on the boundary at the electrically conductive part of the ablation probe.

3. Experimental setup

3.1. Experimental model of RF ablation in ex vivo tissue

Six cadaveric porcine livers (average weight 2300 g) were used for the experiment in room temperature. The RF delivery system was an ELEKTROTOM HiTT 106 generator system (Berchtold, Tuttlingen, Germany) in mono-polar mode, used in conjunction with a single needle 16-gauge cooled-tip ablation electrode. The 12 cm long probe was used. The distal 2 cm of the probe is an electrically conductive metal and the remaining part of the probe is covered with an electrically insulating material to prevent cauterization along the shaft. A grounding pad was applied to the cadaveric liver.

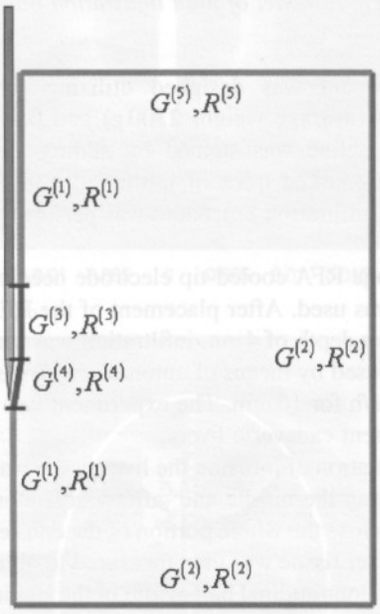

Fig. 6. Boundary conditions applied to the domain.

The RF generator supplies voltage at a frequency of 375 kHz. Ablation treatments were sequentially performed in five predetermined locations in each porcine liver. The probe, inserted into the liver under direct vision to a depth of approximately 4–5 cm, was flushed with normal saline. After insertion of the probe RFA was started while saline at the room temperature (21 °C) was infused at a constant speed of 105 ml/h (as specified by RFA generator manufacturer) using integrated automatic syringe maintaining low tip temperature. Commensurate amount of 35 ml of saline was infused into the liver tissue during every repetitive experiment. After maintaining the baseline power output at 20 W for 1 min, the output was increased to 50 W and RFA was continued for 20 min.

Both the temperature and tissue impedance were monitored during ablation. Temperature data was acquired by type K thermocouple. Two thermocouples were inserted perpendicular to the liver surface. A guiding device that was graduated every 5 mm was used allowing precise placing of the thermocouples. The depth of insertion, reaching the central part of the active probe as calculated according to the length markers of the RFA needle, was controlled using the thermocouple length markers.

The active tips of thermocouples were placed at 5 and 10 mm distance from exposed part of the probe. Temperatures were acquired repeatedly every 1 min using TC-08 thermocouple data logger connected to PC supplied with PicoLog data acquisition software (Pico Technology Limited, Cambridgeshire, UK). All the experiments were repeated at least five times with identical results obtained.

3.2. Experimental model of fluid infiltration into non-viable tissue

The experiment was designed utilizing three cadaveric porcine livers (average weight 2300 g) and 0.9% NaCl solution. Normal saline was stained by adding methylene blue to obtain well-marked trace of infiltrated liquid in cadaveric porcine liver. Infiltration procedure was performed at the room temperature.

The 16-gauge RFA cooled-tip electrode needle with a 2 cm-exposed tip was used. After placement of the RFA needle in a liver tissue at a depth of 4 cm, infiltration was started. The solution was infused by means of automatic syringe at a constant speed of 90 ml/h for 10 min. The experiment was repeated five times in different cadaveric livers.

After termination of infusion the liver tissue was incised longitudinally along the needle and, afterwards, along the needle channel to disclose the whole portion of the colored liver tissue. The colored liver tissue was then measured to obtain transverse half-width and longitudinal half-width of the stained zone. Individual values were recorded accordingly. Average values were calculated as mean with standard deviation.

3.3. Estimation of VSF

Experimental model to determine volume of fluid, which might be injected into certain volume of non-viable tissue, was designed utilizing cadaveric porcine liver and 0.9% NaCl solution at the room temperature. Five liver preparations were excised out of cadaveric porcine liver. Volume of liver preparation was measured by displacement of normal saline in calibrated flask (Archimedes principle).

The 16-gauge RFA cooled-tip electrode needle with a 2 cm-exposed tip was used. After placement of the RFA needle in the liver tissue preparation at a depth of 3–4 cm, infiltration was started. The solution was infused by means of automatic syringe at a constant speed of 90 ml/h for 30 min. The experiments were repeated five times with different cadaveric liver preparations. After termination of infusion volume of infiltrated liver tissue preparation was measured by displacement of normal saline in the same calibrated flask. Individual values of infiltrated liver preparation volume were recorded. VSF, expressed as proportion of infiltrated fluid to liver preparation volume, was calculated accordingly.

3.4. Subsequent experimental validation of the mathematical model of RFA procedure

Further validation of the mathematical model of RFA procedure was accomplished performing 30 additional experiments on cadaveric porcine liver. Local ablations of liver tissue were performed strictly pursuing the protocol, described in Section 3.1. Temperatures were acquired repeatedly every 1 min and were expressed as mean ±SD. All the RFA validation experiments were carried on by an independent researcher (T.V.), who was not involved in the initial experiments.

4. Analysis of results

After performing finite element computational procedure on the model described in Section 2 in *COMSOL Multiphysics* the values of electric potential, electric field strength, temperatures, pressures and other quantities describing the RFA process are obtained at all nodes of the finite element mesh presented in Fig. 7a. Along with contour plots, graph relationships are

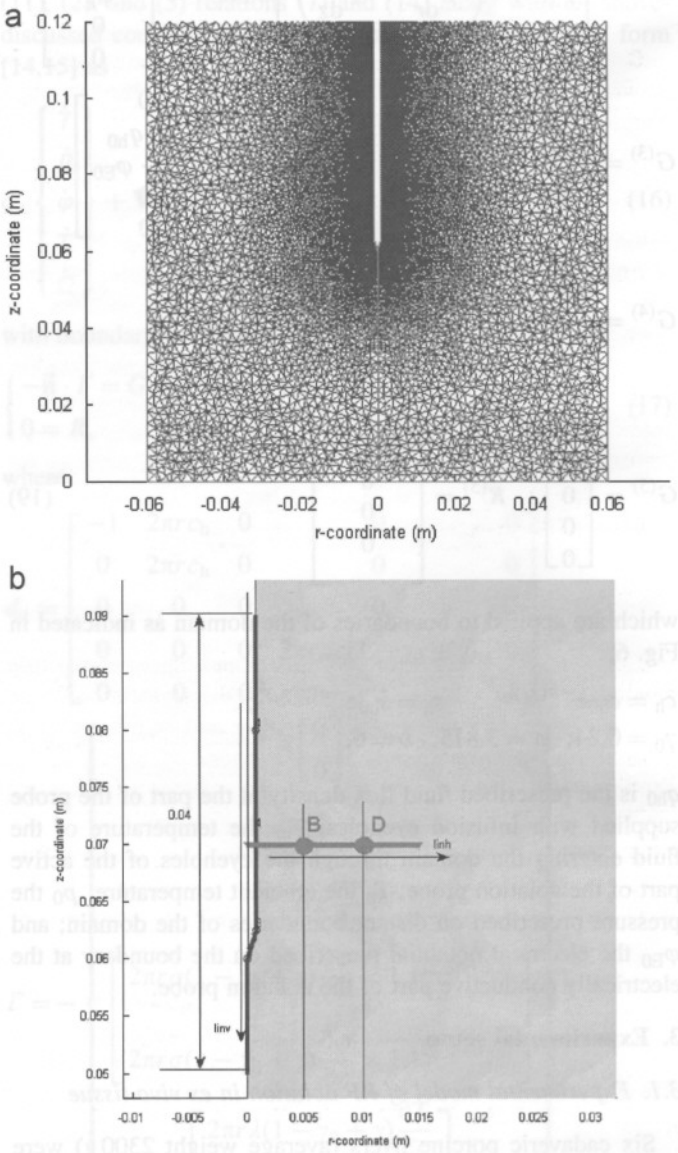

Fig. 7. Finite element mesh containing 19 700 nodes, 38 640 elements. Only the right-hand side represents the computational domain, the other side being geometrically reflected for visualization purposes (a) and reference lines for plotting graph relationships (b).

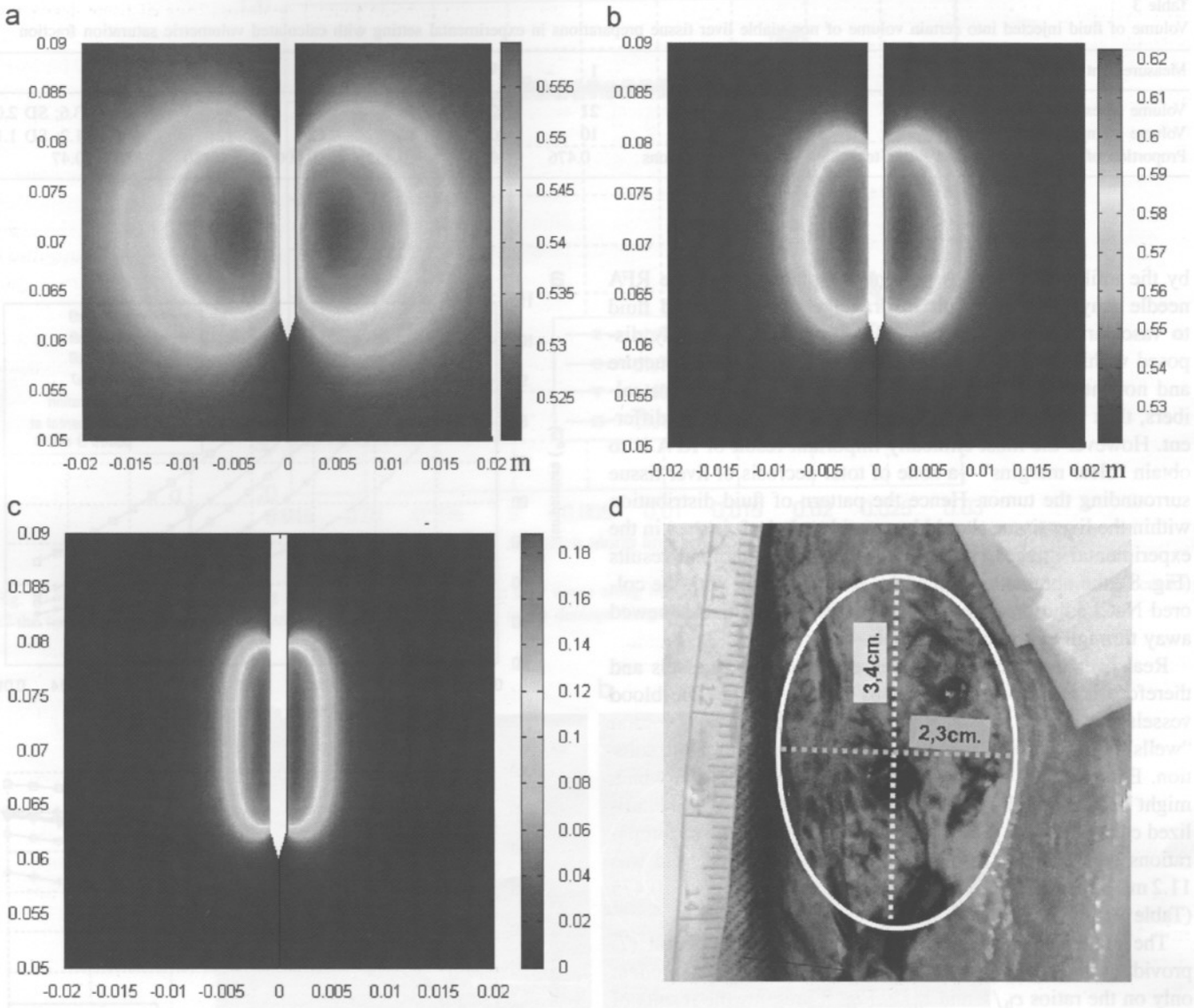

Fig. 8. Distribution of volumetric saturation fraction in the vicinity of the probe after 10 min of injection of colored sodium chloride solution at injection rate 90 ml/h; $s_h/k = 10^6$; $\gamma_0 = 0.84$; $\gamma_{initial} = 0.521$; (a) $(c_h/k) = 10^6$; (b) $(c_h/k) = 5 \times 10^7$; (c) $(c_h/k) = 4.5 \times 10^8$; (d)—experimentally determined zone.

Table 2
Experimental data of porcine liver tissue infiltration by methylene-blue stained saline

Measurement\Experiment	1	2	3	4	5	
Longitudinal half-width of the oval (cm)	3.5	3.4	3.4	3.5	3.6	Mean 3.5; SD 0.1
Transversal half-width of the oval (cm)	1.1	2.3	1.4	1.2	2.2	Mean 1.6; SD 0.6

presented along two selected lines linv (line along the electrically active part of the probe) and linh (horizontal radial line directed outwards from the surface of the probe), Fig. 7b.

The physical constants of the tissue are used as presented in Table 1. The unavailable at the moment constants have been determined by performing reasonably planned physical and numerical experiments.

A physical experiment has been performed, in which methylene-blue stained NaCl solution has been infiltrated into the liver tissue during 10 min time at 90 ml/h injection rate. Fluid infiltration in cadaveric porcine liver produced an irregularly shaped stained zone (Fig. 8d). Mean half-width of longitudinal and transversal dimensions of stained areas, produced in the experimental setting was 3.5 ± 0.1 and 1.6 ± 0.6, respectively. Detailed results of experiments on tissue infiltration are presented in Table 2.

Obtained results enabled us to analyze the geometrical dimensions of stained zone of the tissue, which was reached

Table 3
Volume of fluid injected into certain volume of non-viable liver tissue preparations in experimental setting with calculated volumetric saturation fraction

Measurement\Experiments	1	2	3	4	5	
Volume of excised tissue (ml)	21	22	26	24	25	Mean 23.6; SD 2.07
Volume of injected saline (ml)	10	10	12	12	12	Mean 11.2; SD 1.14
Proportion of volume of injected saline to volume of liver preparations	0.476	0.454	0.462	0.500	0.480	VSF = 0.47

by the infiltrating fluid. A non-guided placement of the RFA needle may possibly result in drainage of the injected fluid to vascular structures. In clinical setting RFA is mainly disposed within the tumor tissue, which is a more solid structure and not intersected with tubular structures of significant calibers, thus fluid distribution within the tumor might be different. However the most clinically important result of RFA is to obtain "clear margins"—a zone of total necrosis of liver tissue surrounding the tumor. Hence the pattern of fluid distribution within the liver tissue should be considered. As it is seen in the experimental images compared against computational results (Fig. 8), the obtained shape of the zone saturated with the colored NaCl solution may be distorted as the solution is sewed away through empty blood vessels.

Real liver tissue contains a dense net of blood vessels and therefore it is a non-homogeneous porous media. The blood vessels are empty in post-mortem liver and serve as natural "wells" able to absorb certain amounts of the injected solution. Experimental model to calculate volume of fluid, which might be absorbed by certain volume of non-viable tissue, utilized cadaveric liver preparations. Mean volume of liver preparations was 23.6 ml. The mean volume of absorbed fluid was 11.2 ml. Analysis of results revealed that mean VSF was 0.475 (Table 3).

The model equations imply that the value of integral (7) providing the VSF values at a point of the model is dependent only on the ratios c_h/k and s_h/k. Fig. 8 presents the results of distribution of VSF in the vicinity of the probe after 10 min of injection.

Tissue saturation mechanism based purely on tissue hydraulic capacity has been assumed by taking $s_h/k = 0$. A deeper consideration and background on this choice may be found in our recent publication [9]. Different values of c_h/k correspond to situations, in which the hydraulic conductance (Fig. 8a) or hydraulic capacity (Fig. 8c) infiltration mechanism was prevailing, as well as, when both of them were significant simultaneously, (Fig. 8b). Results presented in Fig. 8 imply the choice of value $c_h/k \approx 5 \times 10^7$, which ensures the geometrical dimensions of the computed oval zone of the absorbed solution (Fig. 8b) very close to those obtained experimentally (Fig. 8d). In numerical experiments we determined the zone reached by the infiltrating fluid by fixing VSF values $\gamma \geqslant 0.01$.

The Darcy's flow with saturation model can serve only as first and quite rough approximation of the real infiltration process. Nevertheless, the obtained value of equivalent hydraulic conductivity enabled to represent the overall injection and infiltration process satisfactorily.

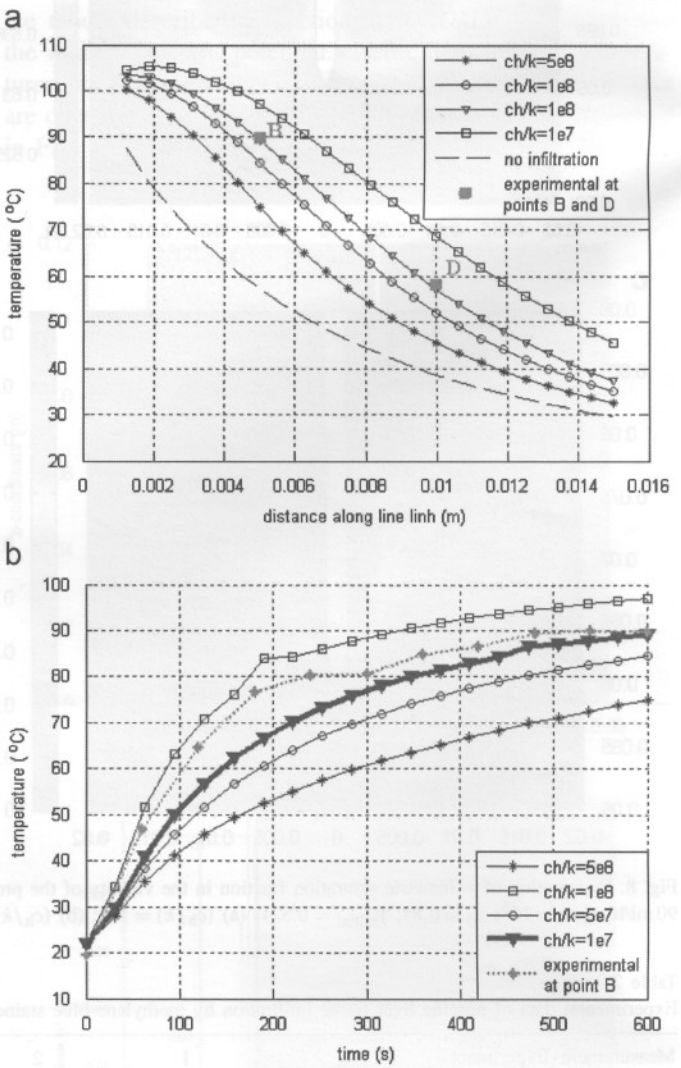

Fig. 9. Temperatures reached during RFA on post-mortem liver tissue at different values of hydraulic capacity of the tissue (no dependence of electrical conductivity against the tissue damage integral taken into account): (a) temperature along line linh at time moment 10 min; and (b) temperature time law at reference point B during first 10 min of RFA process.

On the other hand, the value $c_h/k \approx 5 \times 10^7$ provides a good match of temperature values along line linh (see Fig. 7) at time moment 10 min (Fig. 9a), as well as, during all the time of heating (Fig. 9b). Fig. 10 presents the temperature distribution along line linv at the edge of the ablation probe at different values of c_h/k. It can be seen that value $c_h/k \approx 5 \times 10^7$ again provides realistic results while lower value $c_h/k = 1 \times 10^7$ causes

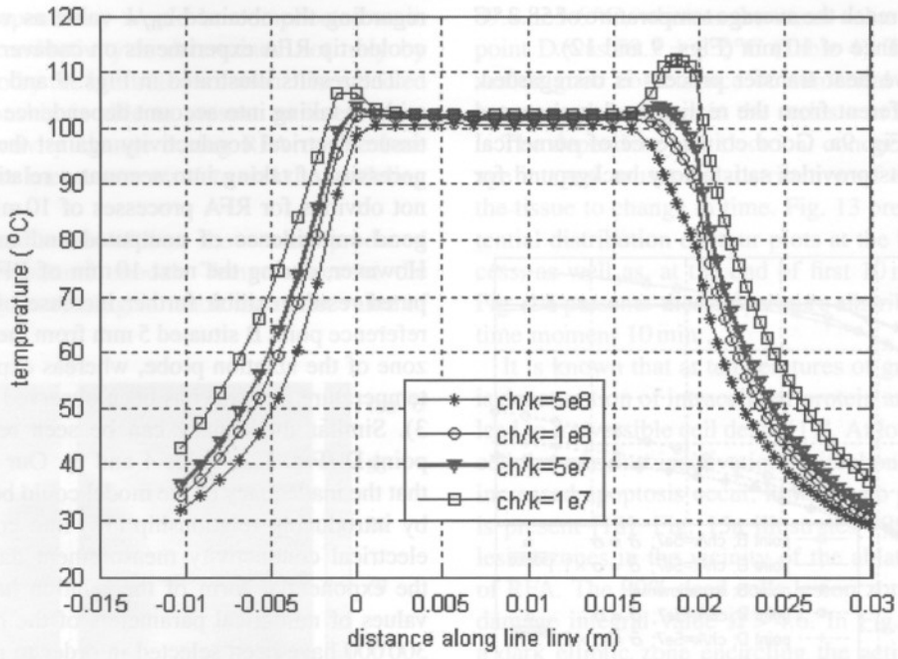

Fig. 10. Temperatures reached during RFA process on post-mortem liver tissue along line linv at time moment 10 min at different values of hydraulic capacity of the tissue (no dependence of electrical conductivity against the tissue damage integral taken into account).

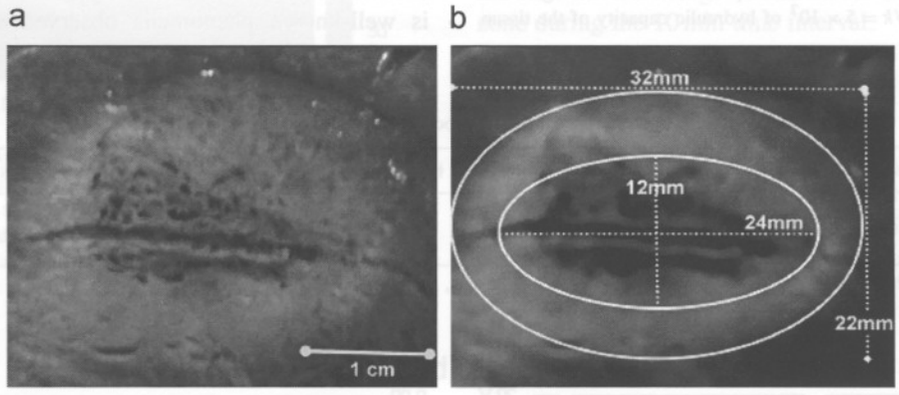

Fig. 11. Lesion zones evaluated according to macroscopic appearance and temperature distribution: (a) macroscopic image of RFA lesion zones; and (b) filtered view of complete (inner elliptic line) and relative (outer elliptic line) lesion zones.

unduly high temperature of the tissue just below the tip of the probe. The temperature of the NaCl solution entering the tissue through the eyeholes of the ablation probe has been assumed as $T_{in} = 100\,^{\circ}C$ and the ambient temperature of cadaveric liver tissue was $T_{amb} = 22\,^{\circ}C$.

Obtaining value c_h/k could be referred to as parameter identification procedure of the model on the base of measured values of temperature at several points over the investigated zone (e.g., as points B and D in Fig. 9a), as well as, on measured time laws of the temperature at selected points during the 10 min interval characteristic for ablation procedures, see Fig. 9b. Practically, we needed to find the model parameters ensuring a good approximation of reference data obtained by measurement. Practical applications of parameter identification procedures sometimes may provide misleading results, if an accidental "mix of model parameters" is found, which enables the modeling results to resemble more or less the results obtained by some particular set of measurements. Fortunately, we can reasonably state that it is not the case here. The computed relationships over space and in time were matched satisfactorily by corresponding measurement results by adjusting the value of single (!) parameter c_h/k during 10 min measurement, where all other model parameters have been taken from known reference sources.

During experimental RFA two oval-shaped zones of tissue destruction were developed: the inner zone of complete lesion and the external zone of relative lesion (Fig. 11a and b) [16]. Temperature rapidly increased for 5 min and stabilized thereafter 5 mm apart from the probe (complete lesion zone) reaching the average temperature of 89.7 °C, whereas it was

gradually increasing to reach the average temperature of 58.2 °C after 20 min at the distance of 10 mm (Figs. 9 and 12).

In case the advective heat transfer process is disregarded, the results are very different from the reality, as demonstrated by the dashed line in Fig. 9a. Good coincidence of numerical and experimental results provides satisfactory background for regarding the obtained c_h/k value as validated for models of cooled-tip RFA experiments on cadaveric liver tissues.

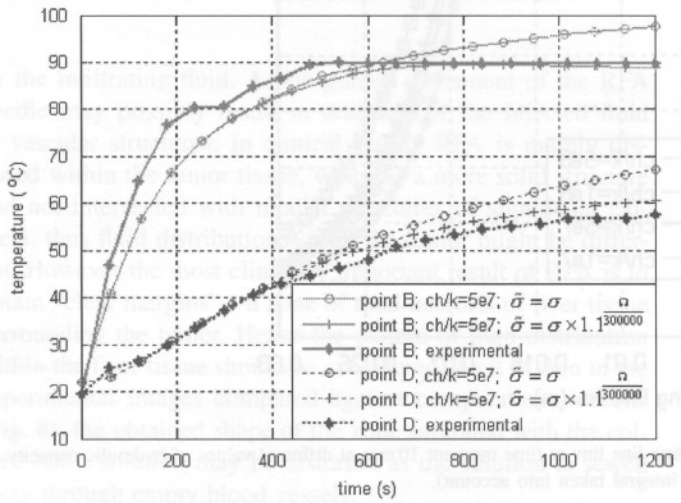

Fig. 12. Temperatures time laws at reference points B and D during 20 min of RFA process at value $c_h/k = 5 \times 10^7$ of hydraulic capacity of the tissue.

The results illustrated in Figs. 9 and 10 have been obtained without taking into account dependence (15), which relates the tissue electrical conductivity against the damage integral. The necessity of taking into account a relationship of type (15) is not obvious for RFA processes of 10 min duration because of good coincidence of computed and measured temperatures. However, during the next 10 min of RFA procedure the computed results exhibit further increase of tissue temperature at reference point B situated 5 mm from the midpoint of the active zone of the ablation probe, whereas experimentally no further temperature increase has been observed (Fig. 12, curves 1 and 3). Similar inadequacy can be seen regarding the results at point D (Fig. 12, curves 4 and 6). Our analysis demonstrated that the inadequacy of the model could be quite simply repaired by introducing relationship (15) into consideration. As direct electrical conductivity measurement data were not available, the exponential form of the relation has been assumed. The values of numerical parameters of the relationship as 1.1 and 300 000 have been selected in order to provide the best match of numerically obtained and experimental results (see Fig. 12, curves 2 and 3 for point B and curves 5 and 6 for point D). The introduced relation (15) is not "artificial" as the decrease of tissue electrical conductivity because of the lesion growth is well-known phenomena observed experimentally. Direct

Table 4
Temperatures obtained after 20 min at the points B and D during validation procedures on cadaveric porcine liver

	Distance from active probe (mm)	Computed temperature (°C)	Experimental results ($n = 30$) Mean ± SD (°C)
Point B	5	89.1	89.8 ± 5.6
Point D	10	60.2	59.3 ± 8.2

Computed temperatures at the points B and D were acquired from calculations, presented in Fig. 12.

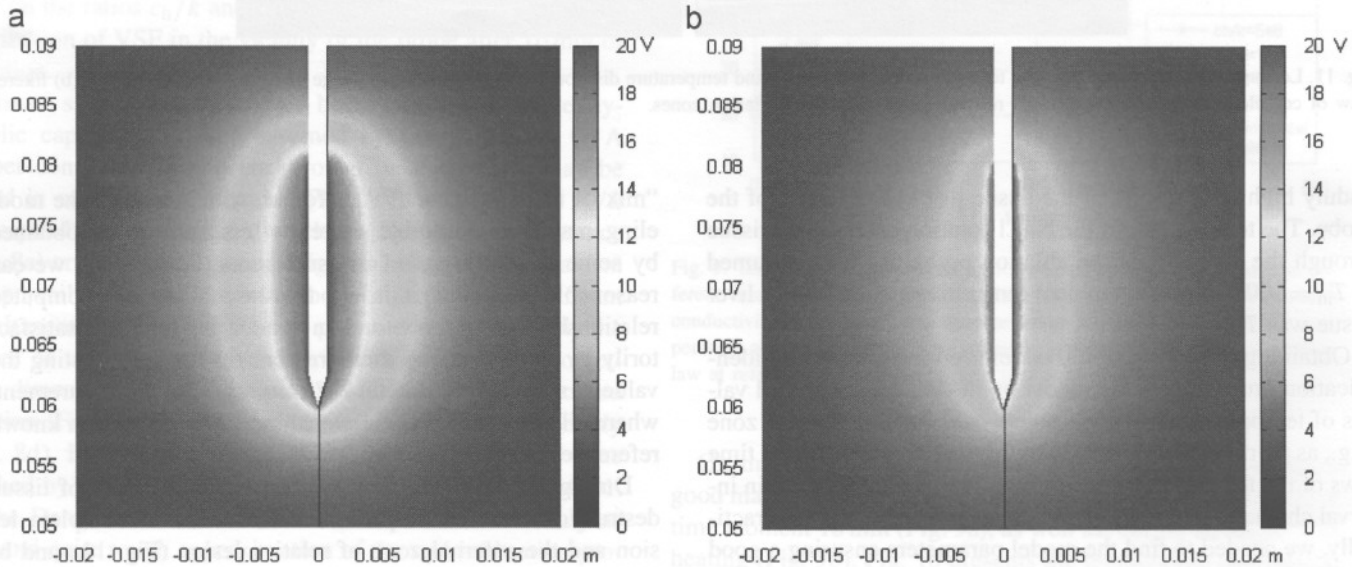

Fig. 13. Distribution of electric potential over the tissue domain in the vicinity of the ablation probe at the start of the RFA process (a) and after 10 min (b) of injection of colored sodium chloride solution at injection rate 90 ml/h. $c_h/k = 5 \times 10^7$; $\gamma_0 = 0.84$; $\gamma_{initial} = 0.521$; dependence (15) of electrical conductivity against damage integral taken into account.

measurement of the dependency would be complicated as in reality the electrical conductivity is determined not only by damaged tissue but also by the infiltrated solution. The selected simple form of relationship is able to present an integral estimation of the conductivity change during RFA on the base of available temperature measurements data and the modeling results.

Subsequent 30 ablated zones of liver tissue were produced to validate the computational model. Temperatures at the point B were gradually increasing to reach the mean value of $89.8 \pm 5.6\,^{\circ}C$, whereas the mean value of temperatures at the point D was $59.3 \pm 8.2\,^{\circ}C$ (Table 4). The results obtained revealed good coincidence of numerical and experimental data as standard deviation in the series was less than 15%.

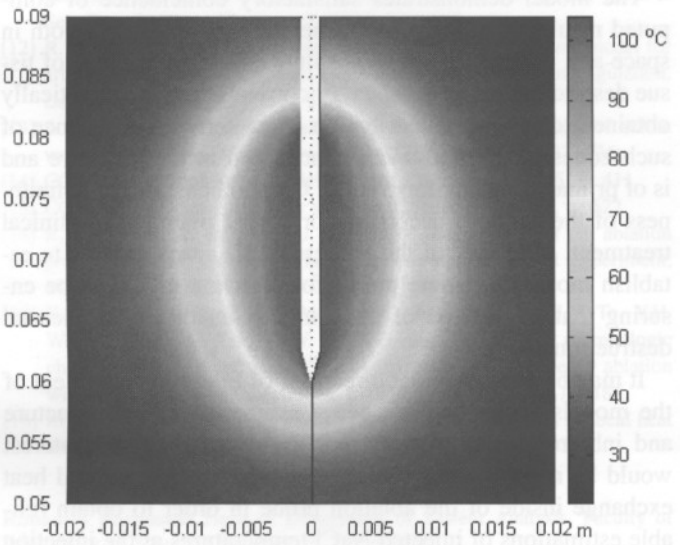

Fig. 14. Distribution of temperature over the tissue domain in the vicinity of the ablation probe at the start of the RFA process and after 10 min of injection of colored sodium chloride solution at injection rate 90 ml/h. $c_h/k = 5 \times 10^7$; $\gamma_0 = 0.84$; $\gamma_{initial} = 0.521$; dependence (15) of electrical conductivity against damage integral taken into account.

The dependency of electrical conductivity against the damage integral causes the distribution of electrical potential over the tissue to change in time. Fig. 13 presents the electrical potential distribution contour plots at the beginning of RFA process, as well as, at the end of first 10 min RFA time interval. Fig. 14 presents the temperature distribution contour plots at time moment 10 min.

It is known that at temperatures of greater than 60 °C, there is denaturation of intracellular protein and lipid bilayers, which lead to irreversible cell death [17]. At lower temperatures intracellular enzyme inactivation, mitochondrial injury, leading to increased apoptosis occur, however no physical tissue damage is present [18]. Fig. 15a illustrates 99% and 63% dead cells lesion zones in the vicinity of the ablation probe after 10 min of RFA. The 99% dead cells lesion zone is determined by the damage integral value $\Omega > 4.6$. In Fig. 14a it can be seen as a dark elliptic zone encircling the active part of the ablation probe. 63% dead cells lesion zone is determined by the damage integral value $1 < \Omega < 4.6$. In Fig. 14a it can be observed as a clearer elliptic ring encircling the 99% zone. Fig. 15b presents the time law of change of half-width of 99% dead cells lesion zone during the 10 min time interval.

5. Conclusion

In this study a finite element model of cooled-tip probe RFA in liver tissues has been developed and investigated. The liver tissue was treated as homogeneous continua. The model describes coupled electric, thermal and NaCl solution infiltration

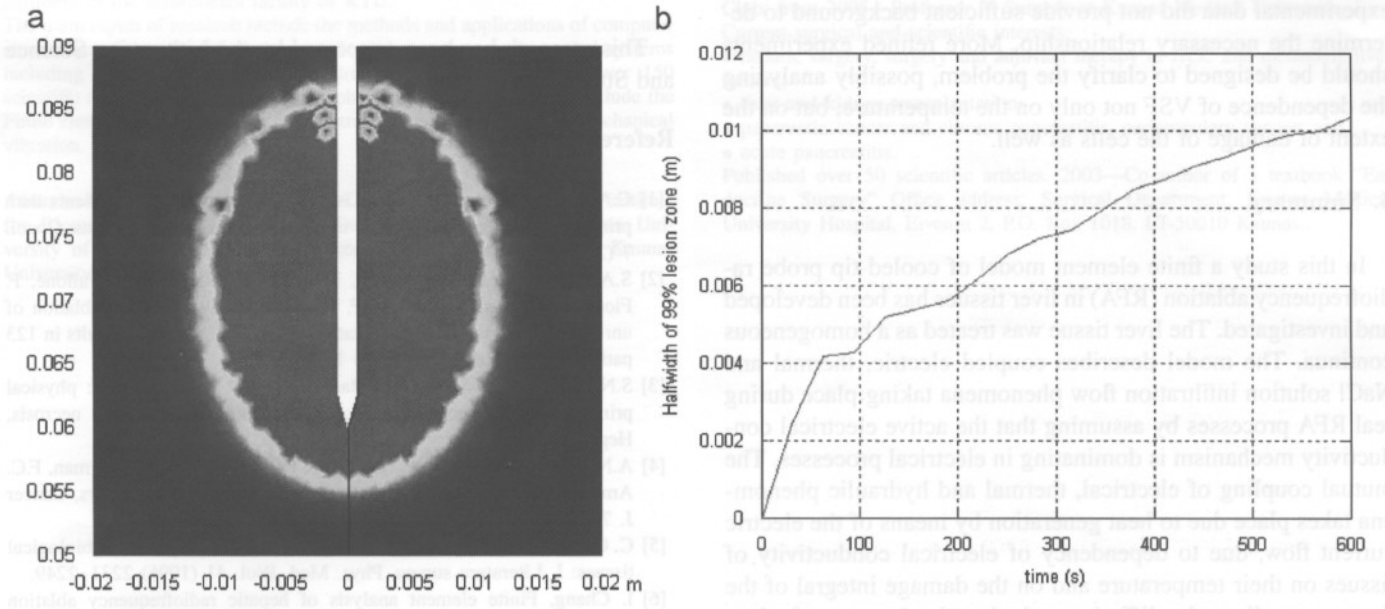

Fig. 15. Lesion zones of 99% and 63% dead cells in the vicinity of the ablation probe after 10 min of RFA (a) and time law of the half-width of 99% dead cells lesion zone (b).

flow phenomena taking place during real RFA processes by assuming that the active electrical conductivity mechanism is dominating in electrical processes. The mutual coupling of electrical, thermal and hydraulic phenomena takes place due to heat generation by means of the electric current flow, due to dependency of electrical conductivity of tissues on their temperature and on the damage integral of the tissue, as well as, the diffusive and advection heat transfer into the tissue. At the same time, an inherent capability of the cadaveric liver tissue to absorb the fluid is taken into account by means of the nonlinear relationship of hydraulic capacity and absorption coefficients against the VSF of the fluid residing in the tissue. The model has been implemented in computational environment *COMSOL Multiphysics*. RFA experiments on porcine liver tissue have validated the model. Based on experimental data unknown physical parameters describing the hydraulic capacity and conductivity in post-mortem liver tissue, as well as, a relation of electrical conductivity of the tissue against the value of damage integral have been determined.

The model demonstrates satisfactory coincidence of computed results against the experimentally obtained data both in space and in time. Observed zones of tissue destruction are in satisfactory correlation with theoretically obtained temperature distribution characteristics. Comprehension and definiteness of the zones is necessary for proper planning of RDA in clinical setting. Modeling of the process in 3D space enables to establish most appropriate points for probe insertion ensuring that all volume of the tumor is inside of the thermal destruction zone.

Directions for future improvement of the models should include better estimation of real structure and inhomogeneity of liver tissue. Another point of interest would be more thorough study of fluid flow process and heat exchange inside of the ablation probe in order to obtain reliable estimations of injected NaCl temperatures at the injection eyeholes of the ablation probe. In this work we also did not take into account the dependence of the VSF from temperature explicitly as our experimental data did not provide sufficient background to determine the necessary relationship. More refined experiments should be designed to clarify the problem, possibly analyzing the dependence of VSF not only on the temperature, but on the extent of damage of the cells as well.

6. Summary

In this study a finite element model of cooled-tip probe radiofrequency ablation (RFA) in liver tissues has been developed and investigated. The liver tissue was treated as a homogeneous continua. The model describes coupled electric, thermal and NaCl solution infiltration flow phenomena taking place during real RFA processes by assuming that the active electrical conductivity mechanism is dominating in electrical processes. The mutual coupling of electrical, thermal and hydraulic phenomena takes place due to heat generation by means of the electric current flow, due to dependency of electrical conductivity of tissues on their temperature and on the damage integral of the tissue, as well as, the diffusive and advective heat transfer into the tissue. At the same time, an inherent capability of the cadaveric liver tissue to absorb the fluid is taken into account by means of the nonlinear relationship of hydraulic capacity and absorption coefficients against the VSF of the fluid residing in the tissue. The model has been implemented in computational environment *COMSOL Multiphysics*.

Comparing numerical results and physical RFA experiments in *ex vivo* liver tissues has validated the model. Unknown physical parameters describing hydraulic capacity and hydraulic conductivity in the tissue, as well as, the relation of electrical conductivity against the value of damage integral have been determined.

The model demonstrates satisfactory coincidence of computed results against the experimentally obtained data both in space and in time. Obtained absolute and relative zones of tissue destruction are in satisfactory correlation with theoretically obtained temperature distribution characteristics. Existence of such zones is reported and characterized in the literature and is of primary clinical importance. Comprehension and definiteness of the zones is necessary for proper planning of clinical treatment. Modeling of the process in 3D space enables to establish most appropriate points for insertion of the probe ensuring that all volume of the tumor is inside of the thermal destruction zone.

It may be supposed that directions of future improvement of the models should include better estimation of real structure and inhomogeneity of liver tissue. Another point of interest would be more thorough study of fluid flow process and heat exchange inside of the ablation probe in order to obtain reliable estimations of injected NaCl temperatures at the injection eyeholes of the ablation probe.

Conflict of interest statement

None declared.

Acknowledgment

This research has been supported by the Lithuanian Science and Study Foundation.

References

[1] C.A. Arciero, E.R. Sigurdson, Liver-directed therapies for patients with primary liver cancer and hepatic metastases, Curr. Treat. Options. Oncol. 7 (2006) 399–409.

[2] S.A. Curley, F. Izzo, P. Delrio, L.M. Ellis, J. Granchi, P. Vallone, F. Fiore, S. Pignata, B. Daniele, F. Cremona, Radiofrequency ablation of unresectable primary and metastatic hepatic malignancies: results in 123 patients, Ann. Surg. 230 (1999) 1–8.

[3] S.N. Goldberg, G.S. Gazelle, Radiofrequency tissue ablation: physical principles and techniques for increasing coagulation necrosis, Hepatogastroenterology 48 (2001) 359–367.

[4] A.N. Mirza, B.D. Fornage, N. Sneige, H.M. Kuerer, L.A. Newman, F.C. Ames, S.E. Singletary, Radiofrequency ablation of solid tumors, Cancer J. 7 (2001) 95–102.

[5] C. Gabriel, S. Gabriel, E. Corthout, The dielectric properties of biological tissues: I. Literature survey, Phys. Med. Biol. 41 (1996) 2231–2249.

[6] I. Chang, Finite element analysis of hepatic radiofrequency ablation probes using temperature-dependent electrical conductivity, Biomed. Eng. Online 2 (2003) 12.

[7] I.A. Chang, U.D. Nguyen, Thermal modeling of lesion growth with radiofrequency ablation devices, Biomed. Eng. Online 3 (2004) 27.
[8] K. Giering, O. Minet, I. Lamprecht, G. Mueller, Review of thermal properties of biological tissues, in: G. Mueller, A. Roggan (Eds.), Laser-Induced Interstitial Thermotherapy, SPIE Optical Engineering Press, Bellingha Washington, 1995, p. 65.
[9] R. Barauskas, A. Gulbinas, G. Barauskas, Finite element modeling and experimental investigation of infiltration of sodium chloride solution into in-vitro liver tissue, Medicina 43 (5) (2007) 399–411.
[10] J. Bear, Dynamics of Fluids in Porous Media, American Elsevier, New York, 1972.
[11] B.-M. Kim, S.L. Jacques, S. Rastegar, S. Thomsen, M. Motamedi, Nonlinear finite-element analysis of the role of dynamic changes in blood perfusion and optical properties in laser coagulation of tissue, IEEE J. Sel. Top. Quantum Electron. 2 (1996) 922–933.
[12] R. Agah, J.A. Pearce, A.J. Welch, M. Motamedi, Rate process model for arterial tissue thermal damage: implications on vessel photocoagulation, Lasers Surg. Med. 15 (1994) 176–184.
[13] A. Strogyn, Equations for calculating the dielectric content of saline water, IEEE Trans. Microwave Theory Tech. 19 (1971) 733–736.
[14] COMSOL Multiphysics, Model Library, Comsol AB, 2005, p. 411.
[15] COMSOL Multiphysics, User's Guide, Comsol AB, 2005, p. 622.
[16] R. Barauskas, A. Gulbinas, G. Barauskas, Investigation of RF ablation process in liver tissue by finite element modeling and experiment, Medicina 43 (4) (2007) 310–325.
[17] K.K. Ng, C.M. Lam, R.T. Poon, T.W. Shek, W.C. Yu, J.Y. To, Y.H. Wo, C.P. Lau, T.C. Tang, D.W. Ho, S.T. Fan, Porcine liver: morphologic characteristics and cell viability at experimental radiofrequency ablation with internally cooled electrodes, Radiology 235 (2005) 478–486.
[18] M. Nikfarjam, V. Muralidharan, C. Christophi, Mechanisms of focal heat destruction of liver tumors, J. Surg. Res. 127 (2005) 208–223.

Rimantas Barauskas Head of Department of System Analysis, Faculty of Informatics of Kaunas University of Technology.
Graduated the Applied Mathematics studies from Kaunas University of Technology (KTU) as Engineer-Mathematician in 1976. Received his PhD (1981) and Habilitation (1992) degrees in Mechanical Engineering at KTU. The focus of research has been computer simulation and analysis of controlled vibration systems with application to vibrations and nonlinear interactions of piezoelectric transducers. Upgraded his knowledge in Technische Hoschschule Aachen, Germany, in 1985–1986 in the field of computational dynamics. During the time period 1994–2001 was the head of Engineering Mechanics Department, and from 2001 until now is the head of System Analysis Department in the Informatics faculty of KTU.
The main topics of research include the methods and applications of computer simulation of the dynamic behavior of solid structures and coupled systems including vibration, impact and penetration problems. Published over 150 scientific articles and several monographs. The teaching activities include the Finite element fundamentals, primary and advanced courses, and Mechanical vibration.

Antanas Gulbinas Head, Laboratory of Digestive System Research, Institute for Biomedical Research; Lecturer, Department of Surgery, Kaunas University of Medicine; Abdominal Surgeon, Department of Surgery, Kaunas University of Medicine Hospital.
1997–1998—Resident Physician, Kaunas 3rd Clinical Hospital, 1998–2002—Resident Surgeon, 2002–2004—Resident Abdominal Surgeon, 2004–2005—Assistant Professor, since 2005—Surgeon and Lecturer, Department of Surgery, since 2005—Head of Digestive System Research Laboratory, Institute for Biomedical Research, Kaunas University of Medicine.
Carries out research in the field of pathogenic mechanisms of liver, pancreas, biliary tract diseases. Publications: Aberrant gata-3 Expression in Human Pancreatic Cancer (J. Histochem. Cytochem., 2006), Inhibition of Heme oxygenase-1 Increases Responsiveness of Pancreatic Cancer Cells to Anticancer Treatment (Clin Cancer Res., 2005), Pancreaticojejunal Anastomosis: the "Achilles Heel" of Pancreaticoduodenectomy (Medicine, Kaunas, 2004), Preoperative Stratification of Pancreas-related Morbidity after the Whipple Procedure (Int. Surg., 2004), Pathogenesis of Pain in Chronic Pancreatitis: Ongoing Enigma (World J. Surg., 2003).
Took professional advancement courses at Aalborg Sygehus, Arhus Univ. Hospital (Aalborg, Denmark, 1997), Inselspital, Universitätsspital Bern (Bern, Switzerland, 2001), Abteilung für Allgemeine, Viszerale und Unfallchirurgie, Universitätsklinikum Heidelberg (Heidelberg, Germany, 2002–2003), Institut für Immunologie und Serologie, Universitätsklinikum Heidelberg (Heidelberg).

Tomas Vanagas In 2001 received a degree from the University of Vilnius, Lithuania. Since 2002 he has been with the Kaunas University of Medicine where he has accomplished residency in abdominal surgery and now is a surgeon at the Department of Surgery.
His research interests focus on pathogenetic mechanisms of liver diseases, local ablative techniques in liver tumors. Publications: Apoptosis is activated in an early period after radiofrequency ablation of liver tissue (Hepatogastroenterol, in press).

Giedrius Barauskas Professor and Chief at Department of General Surgery, Kaunas Medical University Hospital.
1984–1986—Surgical Residency at Kaunas Medical Academy; 1986–1988—General Surgeon at Raseiniai City Hospital, Lithuania; 1989–1995—Assistant Professor in Surgery, 2nd Surgical Clinic, Kaunas Medical Academy; 1993—PhD Thesis on "Long-term Results of Biliodigestive Anastomoses in Benign Biliopancreatic Diseases" (at Kaunas Medical Academy); 1995–1997—Senior Assistant Professor in Hepatobiliary Surgery, Surgical Department, Kaunas Medical Academy Hospital; from 1996—Member in European Digestive Surgery; 1997–2005 Associate Professor in Surgery at Kaunas Medical University; from 2000—Member in IHPBA; from 2001—Member in European Pancreatic Club; from 2001—Consultant for General Surgery at Ministry of Health, Republic of Lithuania; from 2001—Chief, Department of General Surgery, Kaunas Medical University Hospital; from 2004—Member of Scientific Board, European Pancreatic Club; from 2005—Professor in Surgery at Kaunas Medical University.
Current surgical and scientific interests:
- hepatic surgery, surgery and adjuvant therapy in HCC and metastatic liver tumors;
- liver and kidney transplantation;
- pancreatic cancer and chronic pancreatitis, periampulary cancer; and
- acute pancreatitis.

Published over 50 scientific articles. 2003—Co-author of a textbook "Endocrine Surgery" Office address: Surgical Department, Kaunas Medical University Hospital, Eiveniu 2, P.O. Box 1018, LT-50010 Kaunas.